Chapter 8

Frequency-Dependent Optimization of the NaK Ionization Process

In this experiment the central wavelength of the Ti:sapphire oscillator (FS I) was tuned and the dependence of the optimization factors on the excitation/ionization energy was monitored. The NaK ionization process was optimized by applying the already described closed loop scheme (see Chapter 5, section 5.2.3). As a model system the NaK dimer was chosen, as it was intensively studied in our group [20, 50].

The goal of the experiment is to get information about the potential energy curves by changing the photon energy. This is equivalent to Rabitz' proposed inversion problem [6] of using the laser light at different wavelengths in order to scan the potential energy curves (see also Chapter 5, section 5.2.3).

Femtosecond pulse shapes which influence the wave packet dynamics are used in an iterative procedure until the ion signal of NaK is optimized. The ionization takes place in a resonant three-photon step. We have performed optimization experiments between 760 nm and 790 nm. From the modifications of the optimal pulse shapes for different wavelengths one could gain information about the ionization path chosen by the molecular system during the control process. Characteristic motions of the wave packets on the involved electronically excited states are proposed as an attempt to explain the optimized dynamical processes.

Nevertheless, most of the studies are interested only in increasing the efficiency of a particular photo-chemical processes or reactions. The major goal of the presented adaptive control experiments is to gain information about the photo-induced control process itself [109]. The observable is the acquired optimal laser field. This is suitable for this inversion problem, because the

optimal pulse shape should in principle carry all information about the propagation processes of the created wave packets on the involved potential energy curves. Small changes of the laser carrier frequency should allow one to get information about the involved potential curves (if the wave packet chooses different ionization paths). One expects the pulse shape to disclose the best ionization path which is coded within the optimization process. This path may be very sensitive to the tuning of the laser carrier frequency, since other transition states could be also reached within the laser bandwidth. One also expects the ionization efficiency to be influenced by the spectral phase of the pulse shape, since the phase determines the chirp and wave packet interference effects. By applying certain chirps, the wave packet can be guided to propagate along other potential energy curves. For example, it may be produced in an electronic excited state in such a way, that it is refocused later in order to be ionized efficiently or it may be dumped to the electronic ground state in a stimulated Raman process and later pumped back up to the excited state [149]. Constructive interferences of the propagating partial wave packets may occur in the multi-photon process as well, resulting in a higher ionization probability.

8.1 Choice of the System

Alkali dimers are good candidates for this study, since they can be ionized within the wavelength range of commercially available femtosecond oscillators in a 3-photon process. As a model system we have chosen the NaK dimer, because its wave packet dynamics has been already investigated in our group by means of fs pump-probe experiments.

The potential energy diagram of the NaK system is depicted in Figure 8.1, according to Refs. [150, 151]. The electronic states who participate in the pump–probe process are shown. They are the electronic ground state $X(1)^1\Sigma^+$, the bound electronic excited states $A(2)^1\Sigma^+$, $B(3)^1\Pi$ and the ion state $X(1)^2\Sigma^+$. There is a weak spin-orbit coupling between the $A(2)^1\Sigma^+$ and $b(1)^3\Pi$ states [74], which does not strongly influence the real-time dynamics, like e.g. for the K_2 dimer (see Chapter 9).
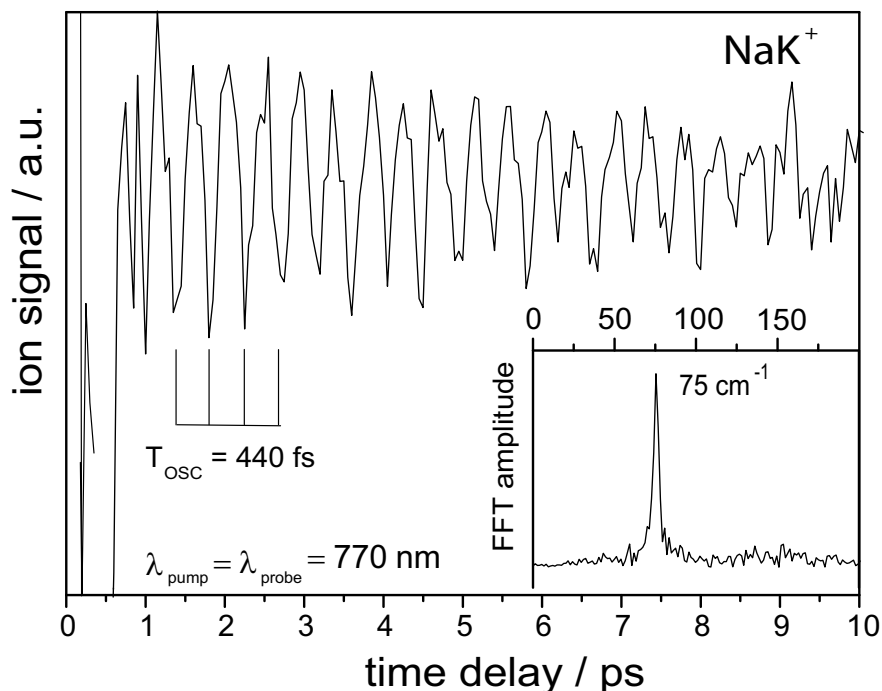
Figure 8.2 shows that the pump–probe spectrum recorded for the NaK molecule exhibits oscillations with a period of $T_{osc}^{NaK} = 440$ fs on the $A(2)^1\Sigma^+$ state [74, 152]. The ionization process takes place in a three-photon step, whereby the central wavelength of both pump and probe pulses is centered around 770 nm.

The pump pulse prepares a wave packet at the inner turning point of the bound electronic excited $A(2)^1\Sigma^+$ state by an one-photon transition. The
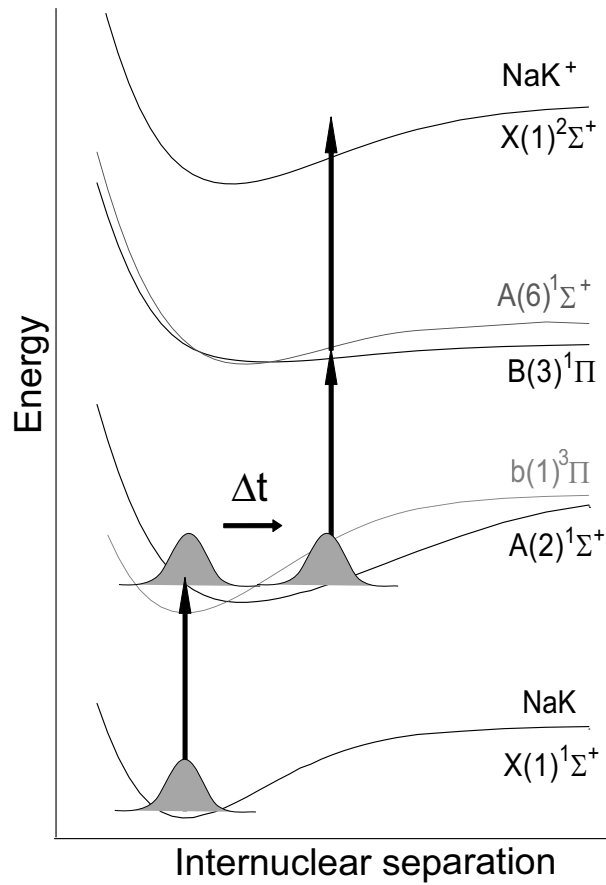
Figure 8.1: Potential energy curves of the heterogeneous NaK dimer (after Refs. [150, 151]). The involved electronic states are the ground state $X(1)^1\Sigma^+$, the excited states $A(2)^1\Sigma^+$, $B(3)^1\Pi$ and the ion state $X(1)^2\Sigma^+$. The pump pulse populates the $A(2)^1\Sigma^+$ and the probe pulse ionizes the system from the outer turning point resonantly via the $B(3)^1\Pi$ state. The oscillation period on the $A(2)^1\Sigma^+$ is $T_{osc} = 440$ fs (see Figure 8.2).

evolution of the wave packet dynamics on the bound state is monitored by the probe pulse, which arrives after a well-defined variable delay time $\Delta\tau$. The probe pulse ionizes the system by a resonant two-photon transition from the outer turning point of the $A(2)^1\Sigma^+$ via the intermediate excited state $B(3)^1\Pi$. The maxima in the pump-probe spectrum represent the effective ionization of the wave packet from the outer turning point of the potential well of the $A(2)^1\Sigma^+$ state performed by the probe pulse. The ionization probability is smaller when the wave packet is situated at the inner turning point (the corresponding minima observed in the time-resolved spectrum). No contribution of the dynamics in the $B(3)^1\Pi$ state was observed in the

Figure 8.2: Time-resolved spectrum of the NaK dimer. The pump and the probe wavelengths were centered at 770 nm. The ion signal exhibits a modulation of the ion signal with a period of 440 fs. The inset shows the Fast Fourier Transform of the pump-probe spectrum. The 75 cm^{-1} component is associated with the frequency of the dimer in the $A(2)^1\Sigma^+$ excited state. This measurement is in agreement with the previous experimental observations of Heufelder [74] and Berg [152].

measured pump–probe spectrum. Nevertheless, theoretical analysis [153,154] state that on the way to the ionic state $X(1)^2\Sigma^+$, the wave packet spends some time on the $B(3)^1\Pi$ state where it vibrates several times.

In the vicinity of zero-time delay between the two pulses, where they overlap, interferences can be observed. The pump and the probe pulses, centered around 770 nm, were delivered by the Ti:sapphire oscillator (80 MHz, 10 nJ, see also section 4.2.1). Its high repetition rate assures a good duty cycle. The experiments take place in the weak field regime where the potential energy curves are not affected by the peak intensity of the laser pulses. Within the focus at the interaction region with the molecular beam the peak intensity of the pulses is estimated to be less than 1 GW cm^{-2}. This will simplify the interpretation of the optimized process.

Certainly, the optimal pulse shapes are usually complicated. Thus one should first investigate simple model systems, e.g. dimers, where the num-

ber of possible pathways is limited. Indications of half and integer values of this period within the optimized pulse shapes would give hints about the ionization path chosen by the optimization procedure.

8.2 Generation of NaK Dimers in Molecular Beams

The NaK clusters are produced in an adiabatic co-expansion of mixed alkali vapor and argon carrier gas through a nozzle of 70 μm diameter into the vacuum. The oven temperature was set to 650°C and the argon pressure to 2 bars. This assures exclusively the production of cold NaK neutral dimers. No trimers or larger clusters are present in the beam, i.e. fragmentation from Na_2K and other larger clusters into NaK is excluded. Thus only the photo-ionization process of the NaK is optimized.

In order to avoid the clogging of the nozzle the temperature around the nozzle region was kept higher by 100 K. As sample commercially available NaK liquid alloy of 99.5 % purity from a sealed ampoule[1] was used. The stagnation conditions of the molecular beam (oven temperature, carrier gas pressure) determine the cluster size distribution. The neutral species pass through the conical-shaped Ni skimmer, which has 1 mm in diameter and is situated 10 mm downstream from the nozzle.

The laser beam is then directed to the cluster beam in order to excite and ionize the neutral particles. The resulting photo-ions are mass-selected by the quadrupole mass analyzer and detected by the secondary electron multiplier (see Chapter 4, section 4.1.3). The stability of the molecular beam during the experiment was monitored by a Langmuir-Taylor detector, which is oriented on the same axis with the nozzle, skimmer and the central region between of the electrical lenses of the mass spectrometer.

8.3 Frequency-Dependent Optimization Factors

In this section the results of the frequency dependent free optimization factors (the ratio of ion yields produced by an optimized and a short pulse I_{opt}/I_{short}, respectively) for the photo-ionization of NaK are presented. The results can be compared when all other parameters (laser bandwidth, pulse energy, molecular beam) are kept as constant as possible. The fluctuations

---

[1]ABCR GmbH & Co. KG, Karlsruhe, Germany.

for each parameter which might influence the results will be given throughout this section.

The constant molecular beam yields a good signal-to-noise ratio and furthermore allows a very high averaging rate. Providing an integration time of about 100 ms, each pulse form is interacting with the molecules about 8 million times. This overcomes laser pulse and molecular beam fluctuations, which are crucial for the analysis of the optimized pulse form.

During the experiments the Ti:sapphire oscillator provided pulses of 100 fs duration (at FWHM) and of about 10 nJ energy per pulse. The laser bandwidth varied by $\pm\,4\,\%$ during the series of experiments. However, the spectral envelope remains the same. The variation in pulse energy is less than 7 % for different central wavelengths. If the fluctuations in the molecular beam were higher than $\pm\,5\,\%$ during an optimization experiment, the measurement was not taken into account.

In the control experiments all the 128 parameters $\Psi_i(\omega)$ of the spectral phase are optimized. This is the most general case when all values are optimized (free optimization). Nevertheless, only the phase of the laser pulse is optimized in order to keep the pulse energy constant. Hence, the transmission of the LC SLM was kept at 100 %. The central wavelength of the oscillator was driven in the range of $\lambda_0=760$–790 nm. The spectral width of the laser during all optimizations was about $\Delta\lambda = 8 \pm 0.3$ nm at FWHM. The short, unshaped pulses exceed the time-bandwidth product by a factor of 1.2, assuming a sech^2 pulse. Thus the spectral phase modulations are comparably small and do not differ noticeably between different center wavelengths [155].

Typically, the learning curve of the optimization algorithm has the form shown in Figure 8.3a for the case of $\lambda_0 = 775$ nm. The curve is obtained by recording the ion yield for each generation. This progression has a similar form for all different laser frequencies. The three curves in Figure 8.3a show the best, the mean and the worst of all values in one generation. At the beginning of the optimization experiment, the ion signal is very low. This is due to the randomly chosen phase values of the first generation. This is expected in a free optimization, since the random phases lead to complex pulse trains which are spread in time over several picoseconds. As a consequence, they produce low ion signals. In the following iterations an enhancement of the NaK$^+$ signal is clearly achieved. The algorithm converges after about 120 generations, when the optimal pulse shape is found.

The mass spectrum in Figure 8.3b shows the distribution of cluster ions when a short pulse is irradiated on the molecular jet. The NaK$^+$ intensity is clearly the most dominant one. The ion signals of the trimers Na$_2$K$^+$, K$_2$Na$^+$ and K$_3^+$ and of other larger clusters are not present in the beam. The ion distribution after optimization is represented in Figure 8.3c. From the
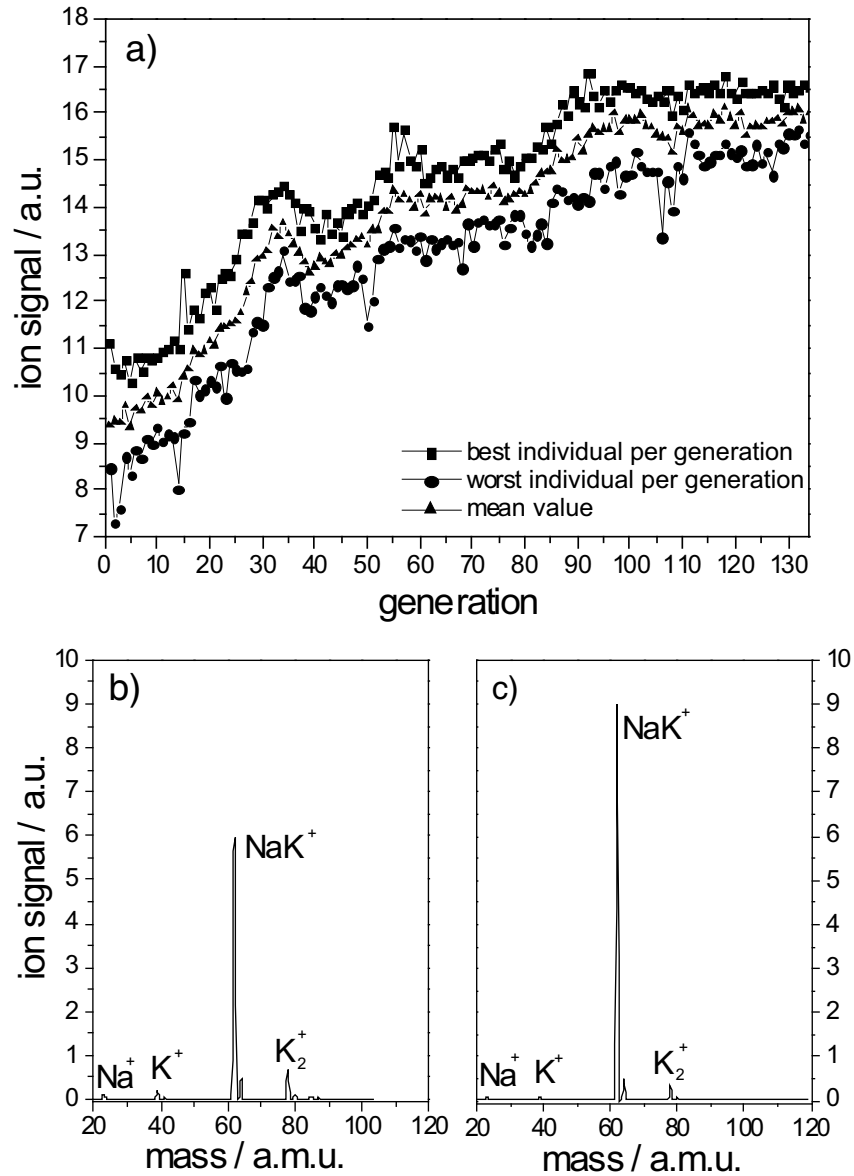
Figure 8.3: (a) Progression of the NaK^+ ion signal during optimization. The laser wavelength is centered at $\lambda_0 = 775$ nm. In the beginning the ion yield is small, since the initial pulses are randomly formed. After approximately 120 iterations the algorithm converges. (b) The mass spectrum recorded with a short pulse exhibits no trimers and larger clusters. (c) The mass spectrum measured with the optimized pulse reveals a NaK^+ yield of $I_{opt}/I_{short} = 1.6$ [155].
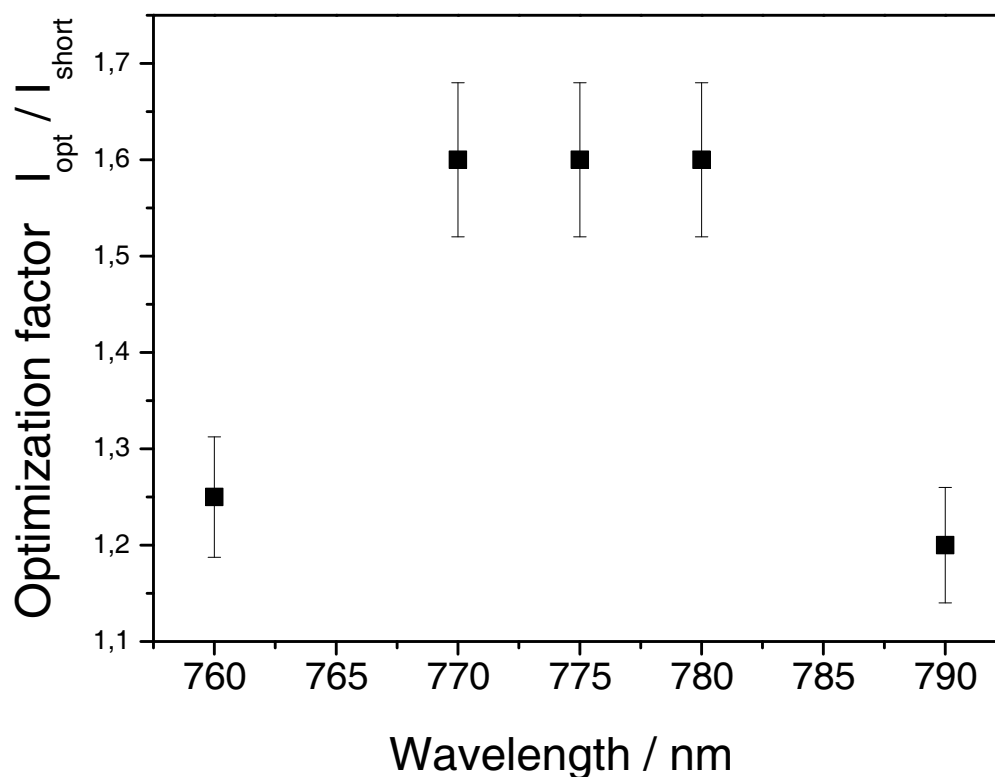
Figure 8.4: Wavelength-dependent optimization factors. The factor is calculated by dividing the ion yield produced by an optimal pulse (I_{opt}) to the ion signal produced by a short pulse (I_{short}) within the experimental error [155].

comparison of the two mass spectra, a rise of about 60 % in the NaK^+ ion yield is obtained. The ion intensities of K_2^+ and K^+ are even smaller after optimization. This can be explained by the fact that the optimal pulse for NaK^+ does not effectively ionize these species.

The noise in the presented optimization curve can be explained by the accidental fluctuations in the cluster beam. One should expect a smooth monotonous rise, since the optimization algorithm leaves the best individual of each generation unchanged (one survivor). As previously mentioned, the molecular beam instabilities were measured to be $\pm$ 5 %. Due to their presence, the best individual in one generation might produce a diminished ion signal in the next generation. This can induce a decrease of the ion signal in the evolution of the best individual, if additionally all other individuals generate less ion yield than the previous best one. Therefore the slight negative variations in the curve of the best values can be understood.
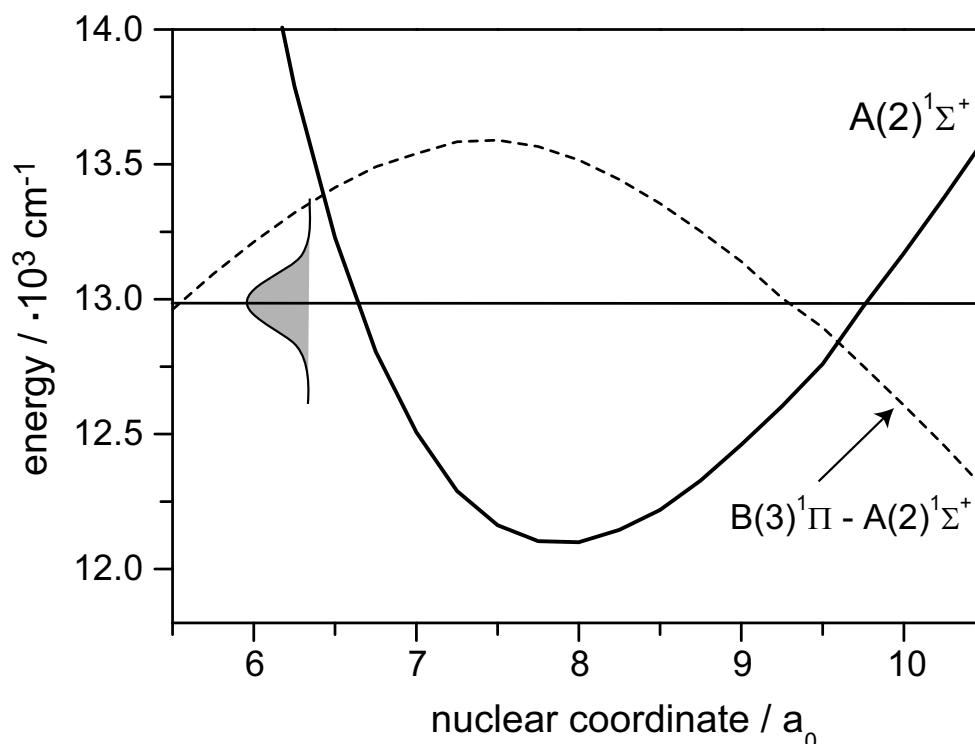
Figure 8.5: The diagram of the involved potential energy curves of the NaK dimer, according to Refs. [150, 151]. The $A(2)^1\Sigma^+$ state and the difference potential $B(3)^1\Pi - A(2)^1\Sigma^+$ cross each other at 12800 cm^{-1} ($\lambda \approx 780$ nm). The spectrum of the laser pulse is indicated as well.

In Figure 8.4 the obtained optimization factors are shown. They are obtained by tuning the central wavelength of the laser between 760 nm and 790 nm. In this graph only the maximal optimization factor recorded for each wavelength is plotted. The reason is that the respective values are obtained for the most stable cluster beam conditions and therefore the least disturbed optimization process. The error bars show the cluster beam fluctuations in determining the optimization factor and not the range of the optimization factors measured for each wavelength.

The graph shows a maximum between 770 nm and 780 nm where optimization factors I_{opt}/I_{short} of 1.6 were measured. The optimization factor decreases to 1.25 at 760 nm and to 1.2 at 790 nm, respectively. Measurements outside this range were not been performed. This is due to difficulties in keeping the laser parameters (FWHM, power, energy) constant. Nevertheless, outside this wavelength region one would expect optimization factors close to 1.

Qualitatively, the graph displayed in Figure 8.4 can be understood by taking into account the involved potential energy curves shown in Figures 8.1 and 8.5. The latter one presents the most relevant part of the NaK potential energy diagram. It shows the first electronic excited state $A(2)^1\Sigma^+$ and the difference potential $B(3)^1\Pi - A(2)^1\Sigma^+$ together with the spectral distribution of the laser pulse at the central wavelength of $\lambda_0 = 770$ nm [150, 151].

The two curves cross each other at an energy of 12800 cm^{-1} ($\lambda \approx 780$ nm), which yields the best resonance condition at the outer turning point for the wave packet propagation in the excited state. Therefore, the optimized ionization path uses this Franck-Condon window in order to achieve the highest ion signal.

At lower photon frequencies, the outer turning point of the wave packet is located more inwards and the $B(3)^1\Pi$ state can not be reached resonantly. This could be reflected in the lower optimization factors obtained at 790 nm.

For higher photon energies the resonance condition to the $B(3)^1\Pi$ state is located at smaller nuclear distances, where the Franck-Condon factors are lower. Furthermore the laser wavelength is closer to the resonance condition for the ionization at the inner turning point, which is more favorable for a short pulse. These facts could lead to a diminished optimization factor at shorter wavelengths.

8.4   Analysis of the Optimal Pulse Forms

In Figure 8.6 the cross-correlation traces of the optimal pulses for 790 nm (a), 775 nm (b), and 760 nm (c), respectively are displayed.

The time-dependent intensity of the optimal pulse shapes for each wavelength is measured by intensity cross-correlation of the optimal pulse with a single, non-optimized pulse. During repeated optimizations the maximized ion yield stays almost the same for different runs. Nevertheless the optimized pulse shapes can slightly differ. The reason could be the high complexity of the parameter manifold (in this case a 128-dimensional searching space), on which the evolutionary algorithm tries to find the best solution. Under the present experimental conditions this solution can be reached by somewhat different pulse structures, since their deviations in fitness are too small to be distinguished. In this section are presented the pulse forms which were frequently obtained for the different frequencies in the optimization runs for the best individual, respectively.

Pulse Form for 790 nm

The cross-correlation for the longest wavelength (Figure 8.6a) reveals a sequence of three intensity maxima[2] with time separations of $\Delta t \approx 250$ fs, a leading pulse located $\Delta t \approx 650$ fs before and an additional trailing pulse $\Delta t \approx 800$ fs after the central triple pulse structure. The intensity ratios of these subpulses amount to 1:6:4:3:1. The subpulse separations $\Delta t \approx 250$ fs can be assigned to half oscillation periods in the excited $A^1\Sigma^+$ state, respectively (see also Figure 8.2). The period of these oscillations was measured to be $T_{osc}^{NaK} = 440$ fs [74], as reproduced by the measurement from Figure 8.2.

In the next paragraph an attempt to give an explanation of the obtained optimized pulse shapes is presented. This is made by taking into account the potential energy curves of the NaK dimer. As mentioned before the applied laser pulses are chosen with a sufficiently low peak intensity in order to work in the weak field regime. This aids our interpretation of the obtained results, since saturation effects can be neglected and perturbation theory can be applied.

The ground state $X(1)^1\Sigma^+$, the excited states $A(2)^1\Sigma^+$, $b(1)^3\Pi$, $B(3)^1\Pi$, $A(6)^1\Sigma^+$ and the ionic ground state $X(1)^2\Sigma^+$ NaK$^+$ are considered for the analysis of optimal photo-induced ionization (see Figure 8.5). Before interaction with the laser field, the system is in the electronic ground state $X(1)^1\Sigma^+$. The first pulse creates a wave packet in the electronic excited $A(2)^1\Sigma^+$ state (see the diagram in Figure 8.7). The wave packet begins to propagate in the potential of the $A(2)^1\Sigma^+$ state. Due to the Franck-Condon principle [67] the wave packet will be created at the inner turning point of the $A(2)^1\Sigma^+$ state and requires $T_{osc}^{NaK} = 440$ fs to return to the starting point [74, 75]. The second pulse arrives after $\Delta t \approx 650$ fs, when the wave packet is located close to the outer turning point. The recorded pump and probe spectrum (see Figure 8.2) shows an enhanced NaK$^+$ ion yield at every $\Delta t = (2n + 1) \cdot 220$ fs between both pulses, i.e. an efficient ionization occurs if the wave packet is situated at the outer turning point of the $A(2)^1\Sigma^+$ state. This transition at the Franck-Condon window takes advantage of the near resonance condition with the $B(3)^1\Pi$ and $A(6)^1\Sigma^+$ state.

In the same time other processes can occur. After excitation from the $A(2)^1\Sigma^+$ state, the population in the $B(3)^1\Pi$ or $A(6)^1\Sigma^+$ state could alternatively be transferred to the ion state by a third pulse. The delayed ionization from this potential can be explained by a doubly excited auto-ionizing state above the ionization threshold. If these states are hit resonantly, the

---

[2]In some of the phrases also the word *subpulses* will be used. It is true that a *subpulse* is defined as a pulse being part of a pulse train. The reader should avoid this apparent semantic confusion.
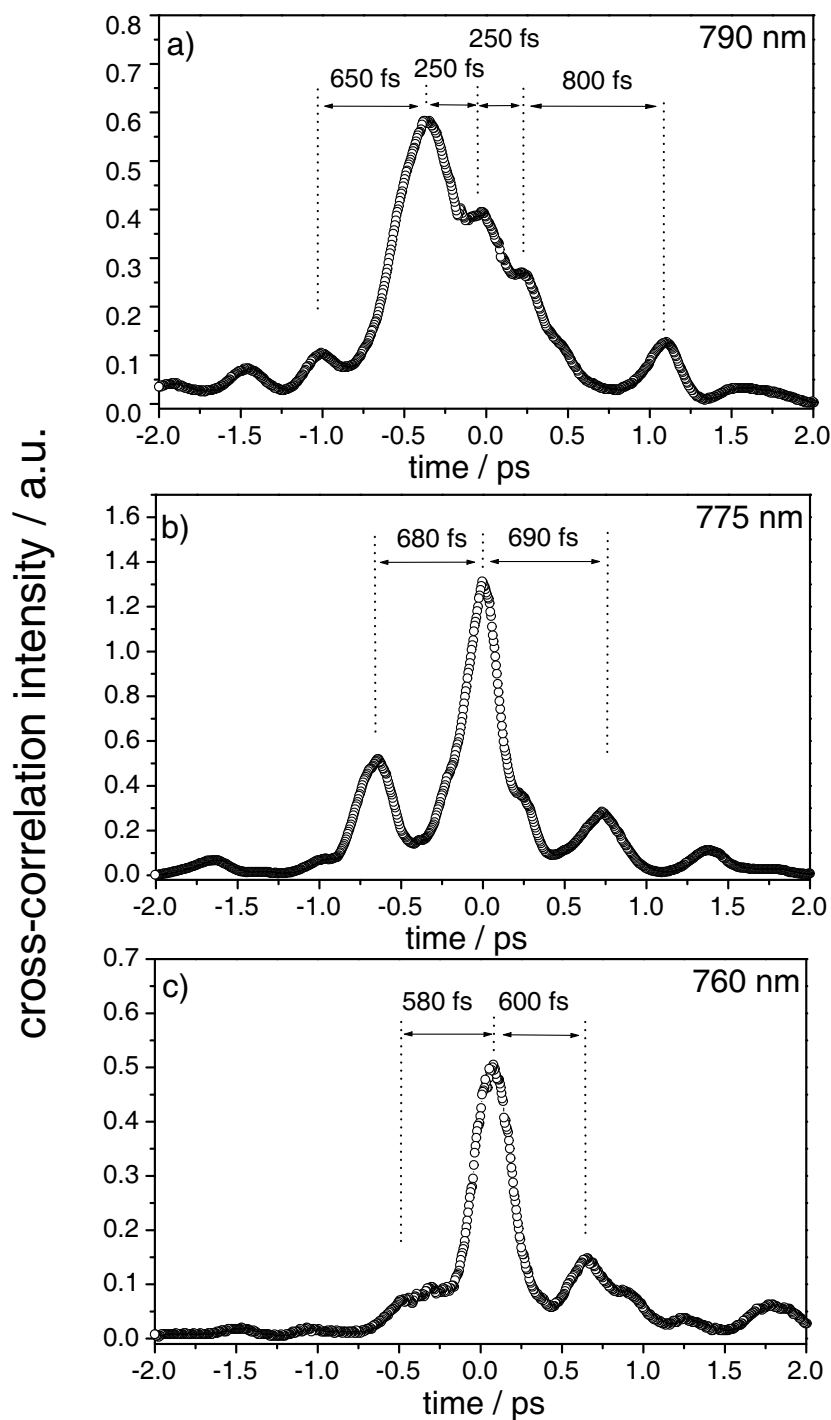
Figure 8.6: Intensity cross-correlations of optimal pulse forms obtained for the ionization of NaK at different central wavelengths: a) 790 nm, b) 775 nm, and c) 760 nm [155].
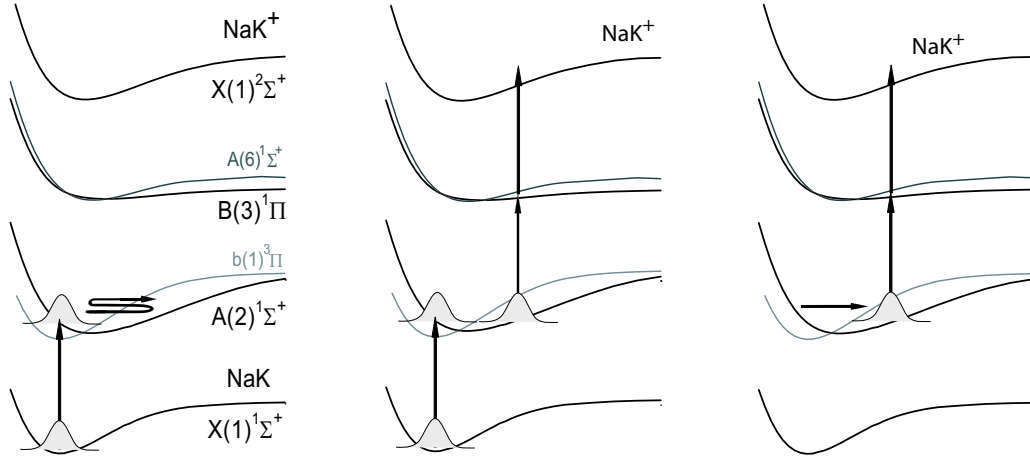
Figure 8.7: Optimal photo-induced ionization path from the ground neutral state of NaK to the ground ionic state of NaK$^+$ via the intermediate excited state(s).

ionization probability increases significantly compared to the excitation into the continuum [156]. As mentioned before the dynamics of a wave packet in the $B(3)^1\Pi$ or $A(6)^1\Sigma^+$ excited states did not contribute to the pump–probe trace from Figure 8.2. Therefore no time dependencies for effective ionization of these states are known. Theoretical calculations performed in the group of Bonačić-Koutecký show that the dynamics in the excited states $B(3)^1\Pi$ and $A(6)^1\Sigma^+$ could also play a role in the optimization process [154].

Since the time separation between the second and third pulse in Figure 8.6a is approximately half of the oscillation period in the $A(2)^1\Sigma^+$ state and the intensity of the second pulse is comparably high, another process is assumed: besides performing ionization, the second pulse can also excite a new wave packet into the $A(2)^1\Sigma^+$ state. The population will be then transferred into the ionic state after $\Delta t \approx \frac{1}{2} \cdot T_{osc}^{NaK}$, as described above. The relative intensities of the subpulses support this interpretation. The excitation step into the $A(2)^1\Sigma^+$ state is performed by the first subpulse via one-photon transition. The second subpulse performs a two-photon ionization and additionally a one-photon excitation into the $A(2)^1\Sigma^+$ state, therefore it is more intense. After 250 fs a third pulse arrives and performs a similar process as the second one. The fourth subpulse, again located 250 fs later, may transfer the residual population to the ionic state via a two-photon process. This sequential process is presented in Figure 8.7. The reason why the evolutionary algorithm has found the last subpulse within the optimization process cannot be explained with this model. The fact that the time separation of the subpulses within the central pulse structure are larger than half

of the oscillation period might be understood by a simultaneous population transfer to the second excited state $B(3)^1\Pi$, which has a longer oscillation period [154]. A trade-off between these two periods, whereby the contribution of the wave packet in the first excited state is dominant, may lead to the observed subpulse spacings.

Pulse Form for 775 nm

The highest optimization factors were obtained after the closed loop optimization experiments at the wavelengths between 770 nm and 780 nm. A typical example of an optimized pulse shape for NaK$^+$ optimization ($\lambda_0 = 775$ nm) is displayed in Figure 8.6b. The pulse shapes recorded for 770 nm (shown in Ref. [149, 157]) and 780 nm are similar in their main structure. This might be due to the partial overlapping of the frequency components at the employed laser bandwidths of $\Delta\lambda = 8$ nm (at FWHM). The cross-correlation trace of this optimal pulse reveals a sequence of three main subpulses separated in time by $\Delta t \approx 680$ fs. The intensity ratios of the pulses are 2:5:1. The time separation of the subpulses $\Delta t \approx 680$ fs can be assigned to one and a half oscillation periods in the electronic excited $A^1\Sigma^+$ state, respectively.

The interpretation of the obtained pulse shape for 775 nm is similar to the one for 790 nm. The first subpulse produces a wave packet in the $A(2)^1\Sigma^+$ state. The second, most intense pulse, arrives at approximately $1.5 \cdot T_{osc}^{NaK}$ later. From here it ionizes the excited molecule at the outer turning point. Additionally it transfers supplementary population from the ground to the first excited state as well. The last subpulse, which arrives later, after $1.5 \cdot T_{osc}^{NaK}$, leads to ionization of the residual population from the $A(2)^1\Sigma^+$ state via the resonant transition state(s).

A few of our optimization runs reveal, like in Ref. [149], a pulse structure for 770 nm, where the splitting between the second and the third subpulse is only half of the oscillation period. This observation demonstrates the limits of our optimization experiment under the given laboratory conditions, since the algorithm is apparently not able to decide between these two solutions, since they have almost equal ionization yields. The fact that, contrary to the case at 790 nm mentioned above, in Fig. 8.6b the time separation between the second and third subpulse is $1.5 \cdot T_{osc}^{NaK}$ and not $\frac{1}{2} \cdot T_{osc}^{NaK}$ may be explained by assuming that the wave packet waits another oscillation period in order to enable a maximal focusing at the outer turning point. The deviation from the case at 790 nm might be caused by the different shape of the wave packet within the excited state, because of the involved energetically higher-lying vibrational states reached by the optimal pulse within the electronic excited

state. The subsequent propagation of the wave packet in the excited state may lead to a more favorable condition after $1.5 \cdot T_{osc}^{NaK}$ for the ionization step compared to the irradiation at 790 nm.

Pulse Form for 760 nm

The pulse shape for the highest photon energy applied in this experiment ($\lambda_0 = 760$ nm) is presented in Figure 8.6c. The cross-correlation trace shows a sequence of two main subpulses separated by $\Delta t \approx 600$ fs and a shoulder $\Delta t \approx 580$ fs before the dominant subpulse. The intensity ratios of the shoulder and the subpulses amount to approximately 1:8:2. The optimized pulse shape shows a similar overall form as the optimal pulse obtained for 775 nm. This case was described above. Due to slightly altered optimal pulse shapes recorded for each optimization experiment, it was not possible to extract a noticeable difference between the pulse forms at these two wavelengths. This reveals the restrictions of our measurements due to the present experimental conditions. Aid from another experimental method, where an initial guess pulse is written on the modulator, or from parametric optimizations with constrains is necessary in order to extract particular features in the optimization process. In order to verify the proposed ionization mechanism, theoretical calculations which will monitor the evolution of the wave packet on the PES induced by the experimentally obtained optimal pulses for each of the employed wavelengths are of an undoubted necessity[3].

8.5   Summary and Outlook

Applying the adaptive feedback control scheme on the model system of NaK, the photon energy dependence of three-photon ionization processes in the alkali dimer was studied. The closed learning loop was used for controlling the wave packet dynamics in the electronic excited states. The shaped femtosecond laser pulses were generated by exclusive spectral phase modulation. The optimization was achieved by maximizing the NaK^+ ion yield.

The dependence of the optimization factors on the employed laser wavelength recorded showed a maximum in the range of 770–780 nm. The recorded pulse shapes reveal information about wave packet propagation at the ionization path, oscillation periods and the involved potential energy curves. For all of the chosen wavelengths three strong subpulses were obtained. The most intense subpulse in the structure of the optimal pulse is predominantly located

---

[3]During this work the experimental and theoretical joint efforts decoded the ionization mechanism performed in NaK by the optimal pulse shapes obtained at 770 nm [153].

at the central position. This has been previously observed in other optimization experiments (see, for example, Refs. [20, 133]). Indications of the excited state oscillation period in the subpulse spacings were found for almost all optimization runs. Changes of the optimal pulse shapes were observed for different wavelengths, revealing modifications of the relative subpulse intensities and spacings within the different applied carrier wavelengths. These optimal pulse shapes offer information about the necessary number of subpulses and their intensities and give additional insight compared with the recent pump-probe experiments of NaK (see section 8.1). Simple models for the ionization pathway were proposed in order to explain the observed features within the pulse shapes. Thereby, only the dynamics in the first excited state $A(2)^1\Sigma^+$ was taken into account. This may oversimplify the interpretation of the optimization process.

By changing the central laser frequency of the femtosecond oscillator, the potential energy curves of the NaK dimer were scanned over an energy range of approximately 500 cm^{-1}. This can be regarded as an automated molecular monitor to explore the involved Hamiltonians, although with the present experimental data this goal cannot be yet reached. By varying the carrier wavelength over a larger spectral range, one would expect a more comprehensive scan of the potential energy curves. If enough experimental data would be available, the potential energy curves could be inferred by solving the inversion problem [6]. The presented approach of learning about the investigated molecular system from the obtained pulse shapes at different photon energies may yield a new way of gaining spectroscopic evidence.

Parametric optimization experiments would give more insight into the ionization mechanism of NaK. By starting with only several laser parameters which are to be optimized, one can follow the course of the optimized ionization process, from the ground state, via the electronic excited state(s), to the ion state. One could take for example, as an initial guess for the evolutionary algorithm, a sequence of three pulses with following parameters per subpulse: spectral FWHM, pulse intensity, the zero-order phase, first-order phase (linear chirp), second-order phase (quadratic chirp), third-order phase (cubic chirp). A pulse sequence consisting of two subpulses would be trivial, since it would reproduce a pump–probe experiment. The temporal separation between two neighboring subpulses can be also an important parameter for the restricted optimization, since it can give hints on the time spend by the wave packet on a particular electronic excited state until the next subpulse arrives.